Nanoscale

Accepted Manuscript

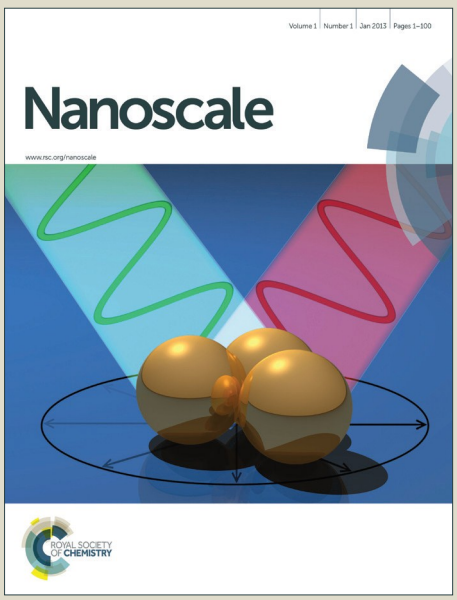

ROYAL SOCIETY OF CHEMISTRY

www.rsc.org/nanoscale

Etching anisotropy mechanisms lead to the morphology-controlled silicon nanoporous structures by metal assisted chemical etching

Bing Jiang[a], Meicheng Li [a,b *], Yu Liang[a], Yang Bai[c], Dandan Song[a], Yingfeng Li [a], Jian Luo[d*]

[a] State Key Laboratory of Alternate Electrical Power System with Renewable Energy Sources, North China Electric Power University, Beijing 102206, China

[b] Suzhou Institute, North China Electric Power University, Suzhou 215123, China

[c] Corrosion and Protection Center, Key Laboratory for Environmental Fracture (Ministry of Education), University of Science and Technology Beijing, Beijing 100083, China

[d] Department of NanoEngineering, Program of Materials Science and Engineering University of California, San Diego, La Jolla, CA 92093, USA

Abstract

The etching anisotropy induced by the morphology and rotation of silver particles controls the morphology of the silicon nanoporous structures, through various underlying complex etching mechanisms. The level of etching anisotropy can be modulated by controlling the morphology of the silver catalyst to obtain the silicon nanoporous structures with straight pores, cone-shaped pores and pyramid-shaped pores. In addition, the structures of helical pores are obtained by taking advantage of the special anisotropic etching, which is induced by the rotation and revolution of silver particles during the etching processing. The investigation of the etching anisotropy of the metal assisted chemical etching will promote the deep understanding the chemical etching mechanism of silicon, and provide a feasible approach to fabricate the Si nanoporous structures with special morphologies.

***Keywords*:** Si nanoporous structures; Etching anisotropy; Rotation of Ag particles; Metal assisted chemical etching.

*Author to whom correspondence should be addressed. FAX: 86-10-61772951. Email:

mcli@ncepu.edu.cn and jluo@alum.mit.edu

1. Introduction

Nanostructures of silicon (Si), which remains the most important material for the current semiconductor industry, are promising building blocks for devices in the field of nanoelectronics[1], opto-electronics[2, 3], energy conversion [4-8] and energy storage[9], as well as bio- and chemical sensors[10, 11]. The characteristic parameters of nanostructures, such as surface and cross-section morphology, orientation relative to the substrate, size and density affect the properties of Si nanostructures and are important for their applications.

Controllable fabrication of Si nanostructures is a prerequisite for their device applications. In recent years, metal-assisted chemical etching (MacEtch) has attracted considerable attention as one facile and cost-effective method for fabricating Si nanostructures with controlled orientation and size features [12-14]. Several prior studies focused on the morphological control of nanoporous Si and Si nanowires through varying the process parameters, such as the oxidant type, etchant concentration, reaction time, processing temperature and type of Si[15-33]. The theory of holes injection during etching is perhaps the most widely accepted mechanism for MacEtch [4, 34-38]. Many observations can be qualitatively explained by the holes' injection from the noble metal particles as the catalyst into the Si substrate and the subsequent diffusion of holes within the Si substrate. For example, diffusion of positive holes from the bottom to the sidewalls can result in the formation of the cone-shaped nanoporous structures and nanowires [13, 18, 20].

In the previous studies, the Si nanostructures etched by MacEtch were considered to be anisotropic along the <111> and <100> directions. Thus, the etching was typically assumed to take place along the vertical <100> on the (100) substrate surface whereas aligned Si nanostructures in (111) or (110) substrate surface [4, 5, 19, 22, 25, 39]. Compared with Si nanowires, the Si

nanoporous structures exhibit more diversiform morphologies and their etching mechanisms appear to be more complex. Besides etching anisotropy, sinking of metal particles, shape of metal particles and distance between the particles also affect the morphology of Si nanoporous structures [15, 31, 34, 40]. However, the exact formation mechanisms of various Si nanoporous structures, including helical, square and cone-shape pores, are not well explained. The effects of the movement of metal particles on the formation Si nanoporous structures remain elusive. Thus, the scientific goal of this paper is to clarify related etching mechanisms via fabricating various Si nanoporous structures by systematically varying several key processing parameters to subsequently achieve mechanism-informed morphological control of Si nanoporous structures.

2. Experimental details

The p-type Si (100) single crystal wafers with resistivity of ρ～7－13 Ωcm were purchased from Emei Semiconductor Factory, China. Single-side polished Si wafers were cut into 1.5 cm × 1.0 cm pieces. Silver nitrate ($AgNO_3$), aqueous ammonia ($NH_3 \cdot H_2O$), glucose ($CH_2OH(CHOH)_4CHO$), hydrofluoric acid (HF, 40%) and hydrogen peroxide (H_2O_2, 30%) were purchased from Sinopharm Chemical Reagent Beijing Company. All the chemicals were reagent grade and deionized water was used to prepare the aqueous solutions of desired concentrations.

The Si samples were cleaned by sonicating in solutions of 40% HF and deionized water. $AgNO_3$ powders were dissolved in the solvent composed of water and ethanol to prepare $AgNO_3$ solutions. The $NH_3 \cdot H_2O$ (0.3M) was continuously dripped into the $AgNO_3$ solution while stirring until the solution became colorless. The 0.2M $[Ag(NH_3)_2]OH$ solution was prepared by mixing appropriate amounts of $AgNO_3$ and $NH_3 \cdot H_2O$ solutions. Then, the cleaned and dried Si samples were placed into the $[Ag(NH_3)_2]OH$ aqueous solution, where the oxidizing $[Ag(NH_3)_2]^+$ was reduced to Ag particles by glucose (0.05M) and deposited on Si surface via the well-known silver

mirror reaction. The morphology of Ag particles on the Si surface can be controlled by the reaction temperature[41]. In this experiment, isolated Ag particles were deposited on the Si substrate via a room-temperature reaction for 5 minutes, while continuous layers of Ag particles were prepared on the Si surfaces by a reaction at 60 °C for 3 minutes.

The isolated Ag particles and continuous Ag layers on the Si surfaces were used as the catalyst to etch Si nanostructures. The etchant solutions are comprised of HF, H_2O_2 and H_2O. Different Si nanoporous structures were obtained by systematically varying the concentration of etchant 1HF:5H_2O_2:10H_2O, 1HF:5H_2O_2:2H_2O, respectively, which are referred to the dilute and concentrated etching solutions in the following text and etching time (5 min, 30 min, 1 hr, 2 hrs and 4 hrs, respectively). Moreover, the isolated Ag particles were used to prepare the helical pores. Then, the formation mechanism of Si helical pores was also investigated by controlling the concentration of HF (40%~90%) (either in dilute or concentrated solutions). The surface and cross-section morphologies of Si pores were characterized by scanning electron microscope (SEM, FEI Quanta 200F).

3. Results and Discussion

3.1 Etching anisotropy induced by different Ag morphology

Previous studies show the etching of Si is intrinsically anisotropic, which can be explained by back-bond breaking theory [4, 34]. Due to the different back-bond strength, it is easier to remove Si atoms on the (100) surface planes, thus, etching occurs preferentially along the < 100 > direction. The vertical nanowires along the <100> direction on the (100) Si surface and the inclined nanowires along the <100> direction on (111) or (110) Si surfaces were evident in previous studies [5, 25]. In our experiments, various Si nanoporous structures are obtained through using either isolated or continuous layers of Ag particles as the catalyst whatever in dilute or concentrated etching solutions.

Figure 1 (a)-(c) shows isolated Ag particles deposited on the Si surface and corresponding Si nanoporous structures that are made using them as catalyst in a dilute etching solution ($1HF:5H_2O_2:10H_2O$). Deep straight pores form after a long etching time of 4 hours, which are typical anisotropic etching structures along the < 100 > direction. Using a concentrated etching solution ($1HF:5H_2O_2:2H_2O$), the similar pores are obtained by isolated Ag particles as the catalyst. Figure 1 (d)-(e) illustrates that still straight pores form and their size and depth increase with increasing etching time. Under this condition, the etching rate is about four times of that when the dilute etching solution is used.

Under the same etching conditions, a ～1 μm-thick, and flocculent, continuous layer of Ag catalyst that is used to make Si nanoporous structures, as shown in Figure 2 (a). Figure 2 (b) and (c) shows that the quasi-square cone pores with rough sidewalls are obtained in the diluted solution. The rough sidewalls in the cross-section image correspond to the stripes in top view image, as shown in Figure 2 (d) and (e). However, in the concentrated solution, cone-shaped and pyramid-shaped pores and porous craters are obtained by applying continuous Ag layers, as shown in Figure 3.

From the results, the different Si nanoporous structures are likely resulted from the different morphology of the catalytic Ag particles whatever in dilute or in concentrated solution. The deep straight pores are obtained by using isolated Ag particles as the catalyst whereas quasi-square cone-shaped pores and inverted pyramid-shaped pores are etched by using continuous Ag layers. The isolated Ag particles have the higher catalytic activity than that of the continuous layers due to the facts that isolated Ag particles are smaller and easier to move around. Therefore, most pores etched by isolated Ag particles are vertical straight pores along the <100> direction because of the drastic etching anisotropy due to high catalytic activity of Ag particles, as shown in Figure 1 (b) and

(c). In the concentrated solution, the combination of high etching rate and the small size of isolated Ag particles drastically intensifies the anisotropic etching, with fast etching along <100> direction to form straight pores, as shown in Figure 1 (d)-(f). However, when the continuous Ag layer are used as catalyst, the difference in etching between the <100> and <111> directions can be observed because of the appropriate catalytic activity due to the continuous morphology of Ag layer. Comparing Figure 1(a) and Figure 2(a), it is evident that the Ag particles in the continuous layer are bigger and denser, and they presumably have lower mobility. Therefore, the etching anisotropy is weakened significantly since the low catalytic activity of continuous Ag layers. In Figure 2 (d), multiple stripes (screw lines) are observed on the sidewalls of the pores, which are likely the footprints left by the rotating Ag particles. Thus, it is considered that the different Si nanoporous structures are ascribed to not only etching anisotropy but also to the movement of Ag particles during etching. Figure 3 (a) shows inverted pyramid-shaped pores that are obtained in concentrated solution, as a result of anisotropic etching between <100> and <111> directions due to the facet etching (Ag layer) instead of point etching (isolated Ag). The four edges of inverted pyramid are induced by preferential etching along the <100> directions, whereas the four triangle facets are originated from the etching along the <111> directions, as depicted in Figure 3 (b). With increasing etching time, Ag particles in the continuous layer partially break loose and sink into the Si substrate to drill pores, and the base of the pores remains square-shaped but their cross-section becomes cone-shaped, as shown in Figure 3 (c). The Si surface is severely etched after 1 hour to become porous crater structures, as shown in Figure 3 (d), which presumably resulted from a secondary etching process (from the subsequent Ag particles that break off from the continuous layer). From above results, the morphology of the Si nanoporous structure is determined by the etching anisotropy and mobility of the Ag particles. The level of etching anisotropy is different when the

Ag particles or layer with different morphology is used as catalyst.

3.2 The rotation of Ag particles for helical pores

In previous studies, helical pores were observed under special etching conditions and could be reduced or eliminated by varying the concentration of oxidant in the etchant[25], which could be presumably resulted from the anisotropic etching rate [40]. In our studies, we observed helical pores with different cross-sectional morphology for the case where isolated Ag particles are used as catalyst in the etching solution with different HF concentration. By contrast, when the Ag layer is used as catalyst, the helical pores cannot be obtained, but some cone-shape or pyramid-shaped pores. Therefore, the helical pores are ascribed to the movement of isolated Ag particles. The underlying mechanisms of forming helical pores via the various modes of coupled particle rotation, revolution, and etching anisotropy are discussed in details.

Figure 4 shows the helical pores with different pitches and shapes, the formation of which is related to the concentration of HF. It is found that 40% is the critical ratio of HF between the straight pores and helical pores. The straight pores are obtained when the ratio of HF is lower than 40% (see Figure 4 (a)). With increasing the ratio of HF above 40%, the helical shape of the pores is more obvious, in which the pitch and width of pores is changing, as shown in Figure 4 (b) - (h). Moreover, it can be seen from the Figure 4 (d) that there are stripes in the sidewall of pore in the top view. In literature, the catalytic activity of metal particles is anisotropic (on the different facet), which is determined by the shape of Ag particles [15, 17, 20, 31, 40]. The helical pore was attributed to the microscopic difference of in etching rate of Si on the Pt particles[40]. Meanwhile, spherical Ag particles are observed in the bottom of pores, which is explained by the dissolution of Ag particles in the etching process [15, 40]. Therefore, the anisotropy should be decreased by the spherical Ag particles due to dissolution in the later etching process. In our studies, the etching

anisotropy induced by the moving path of Ag particles during the etching, as a possible mechanism, is proposed to explain the formation of various helical pores. In a relevant mass transfer model for etching, it is proposed that the Si atoms are oxidized and dissolved at the interface between the metal particles and the Si substrate, and the reagent and byproduct diffuses along this interface[34]. This mechanism is supported by Liu et al.'s etching experiments using anisotropic Pt nanoparticles as the catalyst[31]. Under the lower HF concentration, the Si/Ag interface may be covered with a silicon oxide layer. In this case, the movement of Ag particles is relatively stable and the Si surface can be uniformly etched by positive holes and generate the deep straight pores (see Figure 4 (a)). However, in the solutions with high HF concentration, the oxide layer formed at the Si/Ag interface is thin and easily damaged because the oxide is dissolved at a fast rate. That is, the oxidation and dissolution occur simultaneously. Because of the strong interaction in the Si/Ag interface, the non-uniform etching in Si/Ag interface leads to the Ag particles are under an unbalance surface stress. Moreover, according to the typical anode reaction model, hydrogen could be produced in the interface between Si and Ag particles [34]. In the current experiments, we observed that the samples move around in the etchant when hydrogen is bubbling out from Si surface during the etching procedures. Due to the gravity, surface stress and flowing of hydrogen and reagent, the Ag particles could rotate during the etching procedure. In particular, the rotation direction of Ag particles determines the moving path resulting in the different morphological helical pores. Figure 5 illustrates the relationship between the rotation direction of Ag particles and morphology of different helical pores. When the angle θ is small, the pitch length of the resultant helical pore will be small, as shown in Figure 5 (b). Moreover, all helical pores are found to have the internal stripes in the sidewalls. The observation of the stripes (screw lines) on the inside sidewalls of the pores suggests that Ag particles rotates and etches against the inside sidewalls of the pore during the

etching and sinking process, as shown in Figure 4 (d). Whatever in the concentrated and dilute concentrations, only the concentration of HF is the key factor for the formation of helical pores, resulting in the reaction activities in the interface of Ag particles and Si surface.

Some complex helical pores are also observed in our experiments. Figure 6 (a) shows that several Ag particles gather together under the bottom of a complex helical pore with a large pitch length (HF >40%). When several Ag particles are close to each other, they appear to move in a coordinated path (presumably through the interactions of the stress field) forming this complex, multi-trace, helical pore. However, when the ratio of HF is lower than 40%, this kind multi-trace pores are not helical even though the Ag particles can also move in a coordinated fashion, as shown in Figure 6 (d). Moreover, unique helical pores with Si pillars in the center of the pores are observed, and two examples are shown in Figure 6 (b) and (e). These pores could be induced by the simultaneous rotation and revolution of Ag particles during the etching procedure, and the hypothesized etching process is schematically illustrated in Figure 7. This model shows that when the radius of revolution is larger than the radius of the Ag particles, a Si pillar can remain in the center of the pore (see Figure 7 (b)). The paths of revolution of Ag particles are clearly evident from spiral stripes in the Si pillars, as shown in Figure 6 (b) and (e). The revolution and rotation of Ag particles should be driven by the hydrodynamics in etchant solutions. When these Si pore structures are further etched, the detached helical nanowires are observed, as shown in Figure 6 (c) and (f).

From above results about helical pores, it is proposed that the rotation and revolution of Ag particles plays an important role in the formation of various helical Si nanoporous structures. Therefore, the various helical pores are originated from the concentration of HF, which can induce the rotation and revolution of Ag particles inside the pores during the etching process. In fact, the helical pores induced by rotation or revolution of Ag particles can be as another term of etching

anisotropy.

4. Conclusions

In summary, the morphological control of the silicon nanoporous structures has been achieved upon a systematic utilization of the etching anisotropy in the process of metal assisted chemical etching. The straight deep pores are obtained by isolated Ag particles, whereas the quasi-square and pyramid-shaped pores are induced by continuous Ag layers, which are determined by the different levels of etching anisotropy. The helical pores form as a result of the rotation of Ag particles under the higher HF concentration (>40%). The helical pores with several more complex morphologies, such as entangled multiple spiral pores and helical pores with Si pillars with screw-lines, are ascribed to revolution of Ag particles. The formation of Si helical pores is regarded as another anisotropic etching induced by rotation or revolution of Ag particles. This study demonstrates the feasibility of fabricating the Si porous structures of various morphologies via regulating the etching anisotropy by the morphology and movement of catalytic Ag particles.

Acknowledgement

This work was supported partially by National High-tech R&D Program of China (863 Program, No.2015AA034601), National Natural Science Foundation of China (Grant Nos. 91333122, 51402106, 51372082, 51172069, 51202067 and 61204064), Ph.D. Programs Foundation of Ministry of Education of China (Grant Nos.20120036120006, 20130036110012), Par-Eu Scholars Program, Fundamental Research Funds for the Central Universities and China Scholarship Council. J. Luo also acknowledges partial support from a NSSEFF fellowship (ONR Grant No. N00014-15-1-0030).

Reference

[1] V. Schmidt, H. Riel, S. Senz, S. Karg, W. Riess, U. Gösele, *Small*, 2006, 2, 85-88.

[2] B. Tian, X. Zheng, T.J. Kempa, Y. Fang, N. Yu, G. Yu, et al., *Nature*, 2007, 449, 885-889.

[3] F. Bai, M. Li, P. Fu, R. Li, T. Gu, R. Huang, et al., *APL Materials*, 2015, 3, 056101.

[4] K. Peng, A. Lu, R. Zhang, S.-T. Lee, *Advanced Functional Materials*, 2008, 18, 3026-3035.

[5] Z. Huang, T. Shimizu, S. Senz, Z. Zhang, X. Zhang, W. Lee, et al., *Nano Letters*, 2009, 9, 2519-2525.

[6] F. Hui, L. Xudong, S. Shuang, X. Ying, Z. Jing, *Nanotechnology*, 2008, 19, 255703.

[7] D. Kumar, S.K. Srivastava, P.K. Singh, M. Husain, V. Kumar, *Solar Energy Materials and Solar Cells*, 2011, 95, 215-218.

[8] F. Bai, M. Li, D. Song, H. Yu, B. Jiang, Y. Li, *Journal of Solid State Chemistry*, 2012, 196, 596-600.

[9] K.Q. Peng, J.S. Jie, W.J. Zhang, S.T. Lee, *Applied Physics Letters*, 2008, 93.

[10] Y. Cui, Q. Wei, H. Park, C.M. Lieber, *Science*, 2001, 293, 1289-1292.

[11] F. Patolsky, G. Zheng, C.M. Lieber, *Nature Protocols*, 2006, 1, 1711-1724.

[12] X. Li, P.W. Bohn, *Applied Physics Letters*, 2000, 77, 2572-2574.

[13] F. Bai, M. Li, R. Huang, Y. Li, M. Trevor, K.P. Musselman, *RSC Advances*, 2014, 4, 1794-1798.

[14] F. Bai, M. Li, R. Huang, Y. Yu, T. Gu, Z. Chen, et al., *Journal of Nanoparticle Research*, 2013, 15.

[15] K. Tsujino, M. Matsumura, *Advanced Materials*, 2005, 17, 1045-1047.

[16] D.C. Lim, I. Lopez-Salido, Y.D. Kim, *Applied Surface Science*, 2006, 253, 959-965.

[17] K. Tsujino, M. Matsumura, *Electrochimica Acta*, 2007, 53, 28-34.

[18] C. Chartier, S. Bastide, C. Lévy-Clément, *Electrochimica Acta*, 2008, 53, 5509-5516.

[19] C.-Y. Chen, C.-S. Wu, C.-J. Chou, T.-J. Yen, *Advanced Materials*, 2008, 20, 3811-3815.

[20] C.-L. Lee, K. Tsujino, Y. Kanda, S. Ikeda, M. Matsumura, *Journal of Materials Chemistry*, 2008, 18, 1015-1020.

[21] Y.M. Yang, P.K. Chu, Z.W. Wu, S.H. Pu, T.F. Hung, K.F. Huo, et al., *Applied Surface Science*, 2008, 254, 3061-3066.

[22] M.-L. Zhang, K.-Q. Peng, X. Fan, J.-S. Jie, R.-Q. Zhang, S.-T. Lee, et al., *The Journal of Physical Chemistry C*, 2008, 112, 4444-4450.

[23] O.J. Hildreth, W. Lin, C.P. Wong, *ACS Nano*, 2009, 3, 4033-4042.

[24] M.L. Chourou, K. Fukami, T. Sakka, S. Virtanen, Y.H. Ogata, *Electrochimica Acta*, 2010, 55, 903-912.

[25] Z. Huang, T. Shimizu, S. Senz, Z. Zhang, N. Geyer, U. Gösele, *The Journal of Physical Chemistry C*, 2010, 114, 10683-10690.

[26] X. Geng, M. Li, L. Zhao, P.W. Bohn, *J Electron Mater*, 2011, 40, 2480-2485.

[27] S.-C. Shiu, S.-B. Lin, S.-C. Hung, C.-F. Lin, *Applied Surface Science*, 2011, 257, 1829-1834.

[28] S. Yae, Y. Morii, N. Fukumuro, H. Matsuda, *Nanoscale Research Letters*, 2012, 7, 352-358.

[29] J. Cichoszewski, M. Reuter, F. Schwerdt, J.H. Werner, *Electrochimica Acta*, 2013, 109, 333-339.

[30] N. Geyer, B. Fuhrmann, H.S. Leipner, P. Werner, *ACS Applied Materials & Interfaces*, 2013, 5, 4302-4308.

[31] G. Liu, K.L. Young, X. Liao, M.L. Personick, C.A. Mirkin, *Journal of the American Chemical Society*, 2013, 135, 12196-12199.

[32] A. Backes, U. Schmid, *Sensors and Actuators B: Chemical*, 2014, 193, 883-887.

[33] F. Bai, M. Li, R. Huang, D. Song, B. Jiang, Y. Li, *Nanoscale Res Lett*, 2012, 7, 1-5.

[34] Z. Huang, N. Geyer, P. Werner, J. de Boor, U. Gosele, *Advance Materials*, 2011, 23, 285-308.

[35] C.-Y. Chen, C.-P. Wong, *Chemical Communications*, 2013, 49, 7295-7297.

[36] C.Q. Lai, H. Cheng, W.K. Choi, C.V. Thompson, *The Journal of Physical Chemistry C*, 2013, 117, 20802-20809.

[37] Z.R. Smith, R.L. Smith, S.D. Collins, *Electrochimica Acta*, 2013, 92, 139-147.

[38] R. Douani, K. Si-Larbi, T. Hadjersi, N. Megouda, A. Manseri, *Physica Status Solidi (a)*, 2008, 205, 225-230.

[39] H. Chen, H. Wang, X.-H. Zhang, C.-S. Lee, S.-T. Lee, *Nano Letters*, 2010, 10, 864-868.
[40] K. Tsujino, M. Matsumura, *Electrochemical and Solid-State Letters*, 2005, 8, C193.
[41] B. Jiang, M. Li, D. Song, Y. Li, T. Mwenya, *Crystal Research and Technology*, 2013, 48, 1044-1049.

Figure Captions

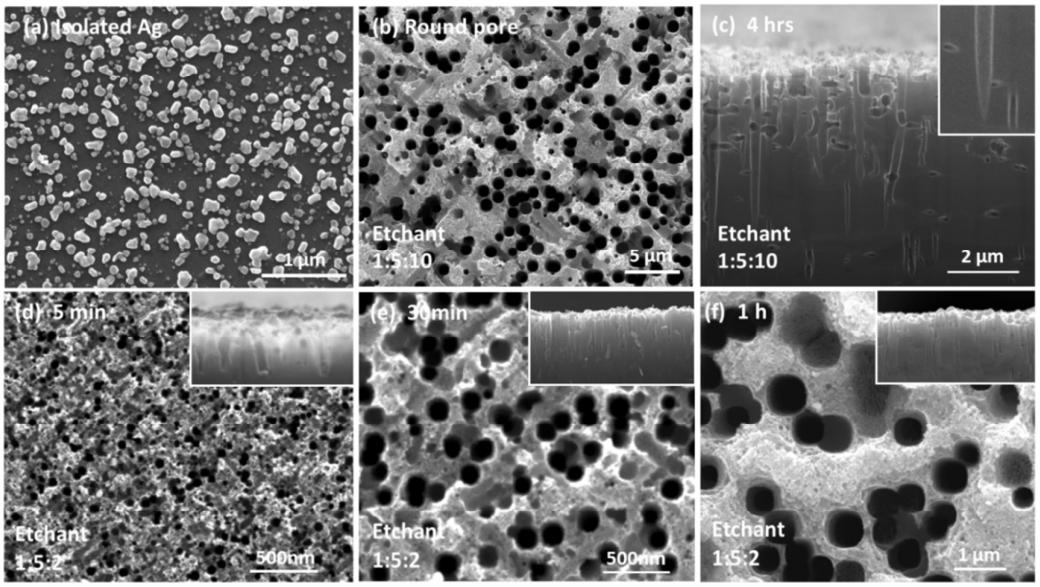

Figure 1 SEM micrographs of (a) isolated Ag catalyst particles on the surface of a Si wafer and (b) the Si nanoporous structure obtained after etching in a dilute $1HF:5H_2O_2:10H_2O$ solution for 4 hours and (c) the corresponding cross-section morphology; (d) the Si nanoporous structure obtained after etching in a concentrated $1HF:5H_2O_2:2H_2O$ solution for 5 mins, (e) 30 mins and (f) 1 hours. The insets show the corresponding cross-section of the pores.

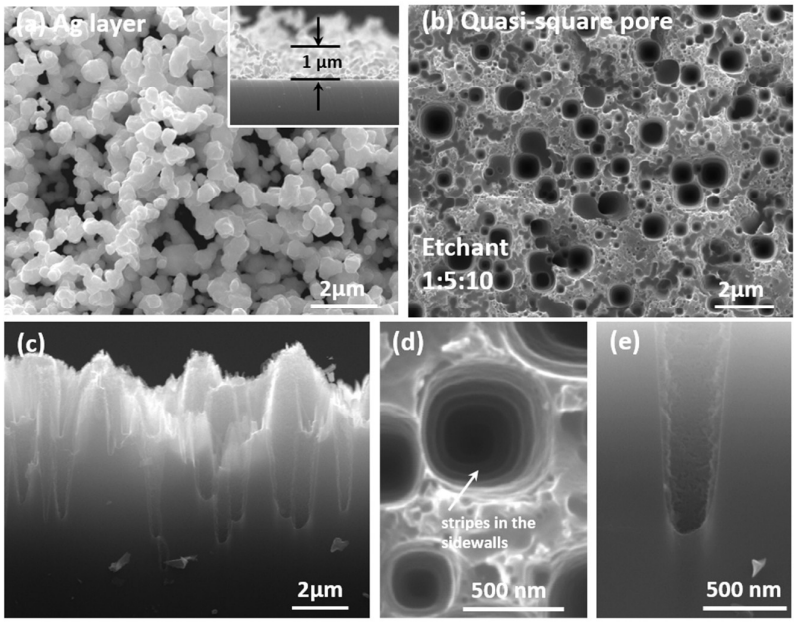

Figure 2 SEM micrographs of (a) a continuous layer of Ag catalyst and (b) the Si quasi-square, cone-shaped pores obtained after etching in a dilute 1HF:5H_2O_2:10H_2O solution for 4 hours using the catalyst shown in panel (a). Additional SEM micrographs of (c) a cross-section of the Si nanoporous structure, (d) an enlarged view of quasi-square pores with screw lines on the insight surface, and (e) a cross-section showing that the pore has a cone shape with a rough surface.

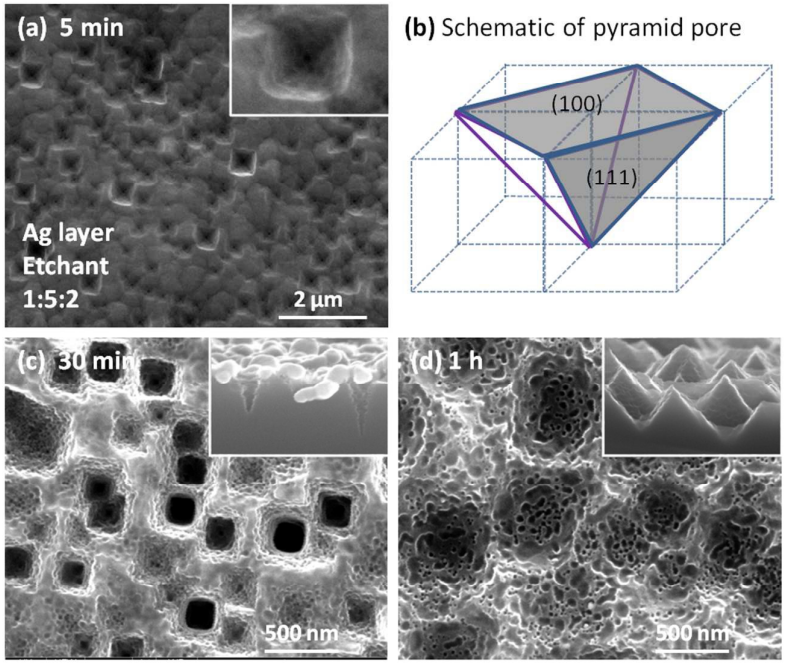

Figure 3 SEM micrographs of the square pyramid-shaped pores etched in a concentrated 1HF : 5H_2O_2: 2H_2O solution using continuous layers of Ag catalyst particles for (a) 5 minutes, (c) 30 minutes, and (d) 1 hour, respectively. The insets are the corresponding cross-sectional morphology. A schematic of the inverted pyramid pore is shown in (b).

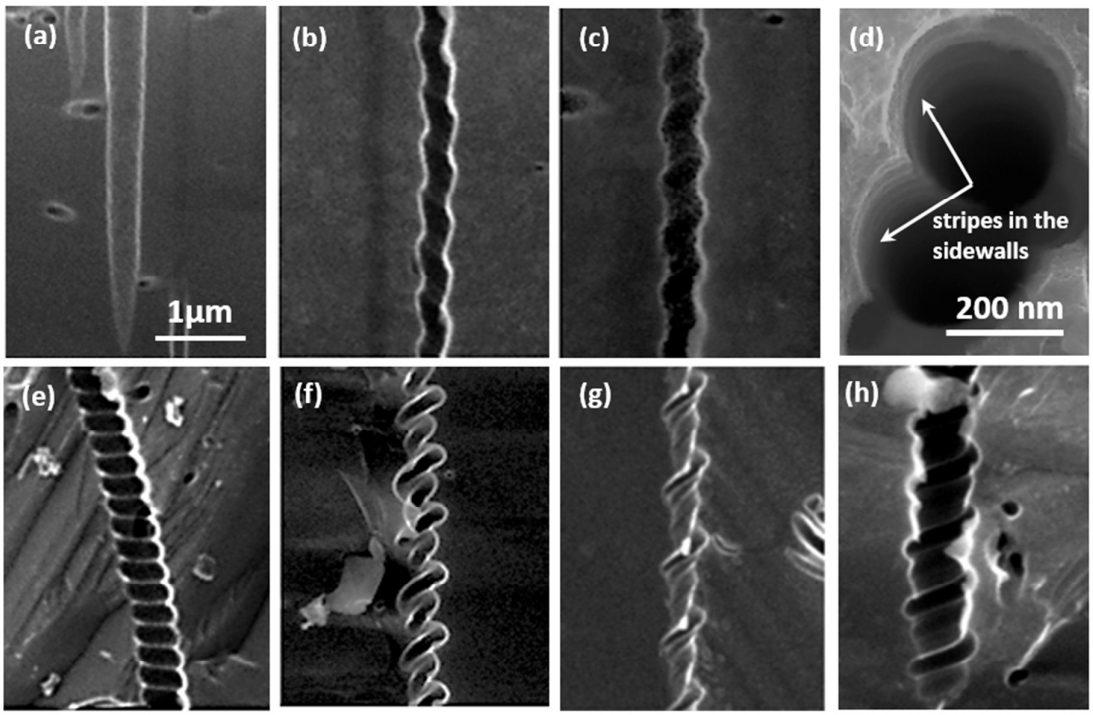

Figure 4 Cross-sectional SEM micrographs of helical pores with different morphologies etched by isolated Ag particles. (a) 16.7% HF (b) and (c) 40% HF (d) an enlarged top view of helical pores under the 50% HF (e) 50% HF (f) 83.3% HF (g) and (h) 90% HF.

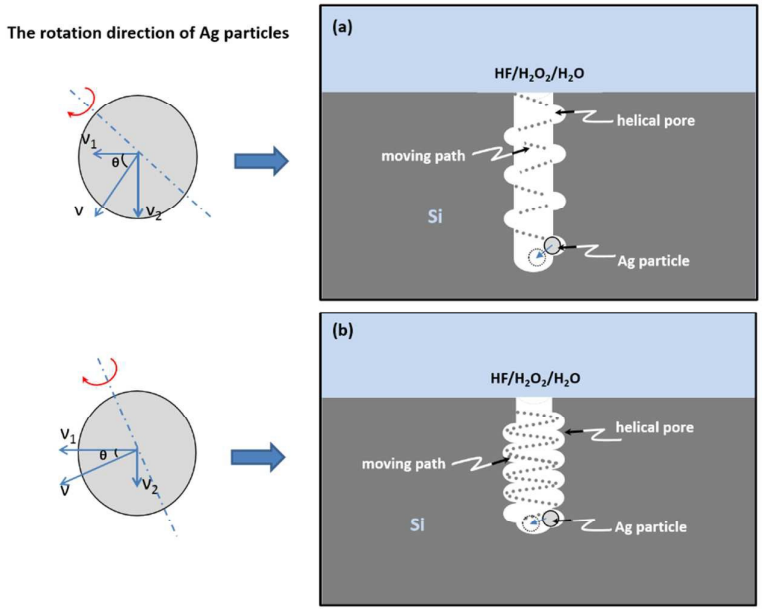

Figure 5 Schematic illustration of the rotational direction and probable moving paths of Ag particles and during the process of forming helical pores with different pitch and width.

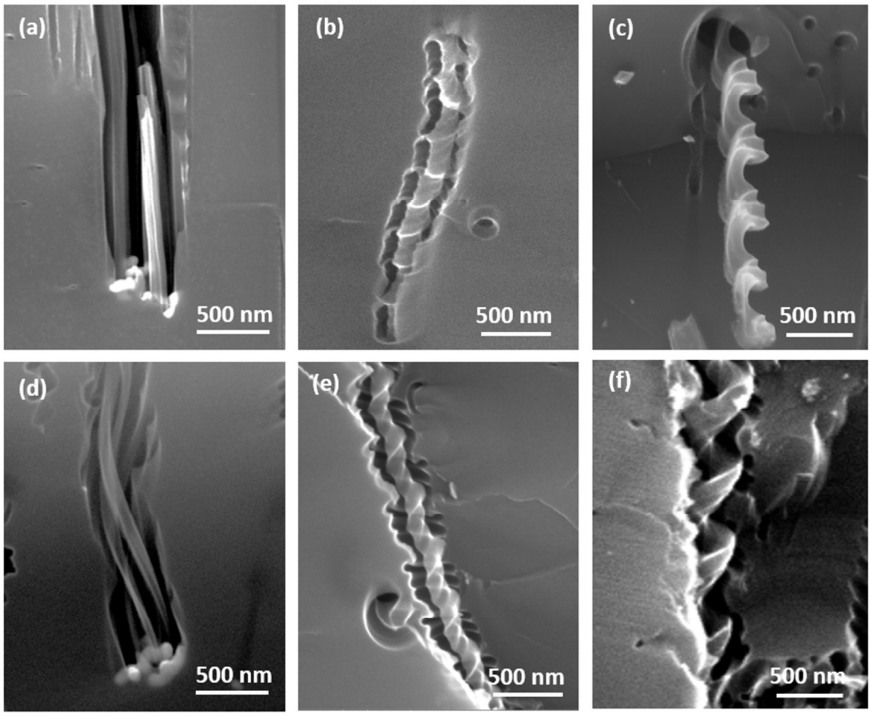

Figure 6 Cross-sectional SEM micrographs of several helical pores with complex morphologies. (a, d) entangled multiple pores; (b, e) helical pores with the screw-line Si pillar in the centers; (c, f) helical bend nanowires detached from the pores.

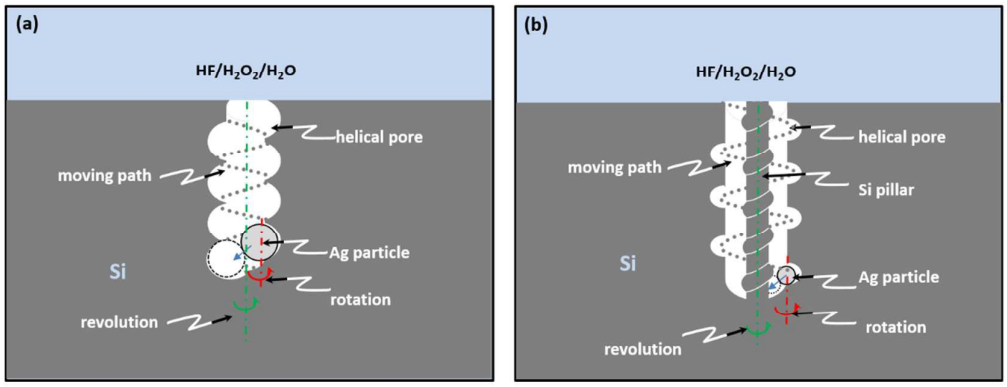

Figure 7 Schematic illustrations of the formation of (a) normal helical pore and (b) helical pores with screw-line Si pillar in the center.